

The Effect of Melt Conditioning on Segregation of Solute Elements and Nucleation of Aluminum Grains in a Twin Roll Cast Aluminum Alloy

KEEHYUN KIM

An aluminum alloy was cast by a laboratory scale horizontal twin roll caster with or without melt conditioning by the intensive shearing prior to solidification and then examined by high-resolution electron microscopy. The combined twin roll casting process with solidification formed channels and induced centerline segregation without the conditioning. In comparison, the melt conditioning minimized the severe segregation on the surface as well as at the centerline. Furthermore, large amounts of solute elements were uniformly distributed along grain boundaries or interdendritic regions. Analytical electron microscopy detected a fine oxide particle or a fragmented aluminum particle particularly at the center region of one nucleated aluminum grain. In addition, large oxide particles of about 1 to 5 μm nucleated aluminum grains easily due to low undercooling necessary for the heterogeneous nucleation, whereas small oxides with the size of about 100 to 200 nm requiring large undercooling were pushed along the grain boundaries instead of contributing to the nucleation. The enhanced nucleation of aluminum grains and well-distributed solute atoms in the melt by the melt conditioning resulted in the minimization of macro- and micro-segregations and the formation of a uniform microstructure.

DOI: 10.1007/s11661-014-2414-y

© The Minerals, Metals & Materials Society and ASM International 2014

I. INTRODUCTION

A fine grain size and structural uniformity has generally favorable mechanical properties of most metals and alloys.^[1] In casting, fine equiaxed grains are important for the service performance of cast products and final properties of semifabricated products by the reduced ingot cracking, improved shrinkage porosity, and well-distributed second phases.^[2-4] In particular, the fine grains reduce the hot cracking sensitivity of an alloy due to evenly distributed strains.^[5] For over half a century, in order to achieve such a fine microstructure in aluminum alloys, inoculants of micrometer size, such as TiB_2 , TiC , or TiAl_3 , have been added to aluminum melt with additional titanium to act as substrates for heterogeneous nucleation of aluminum grains during solidification and consequently in order to enhance the nucleation.^[6-8]

Although the inoculants improve the properties, several problems are encountered with them through the loss of performance over time by agglomeration, settling or poisoning, and formation of undesired particles.^[9,10] Recently, however, it has been suggested that a melt conditioning (MC) process can achieve a grain-refined microstructure without adding any exogenous particles. Depending on the method generating the shearing of melt,

the process is divided into four main groups: (1) twin screws,^[9,11-14] (2) rotor-stator unit,^[15,16] (3) electromagnetic stirring,^[17-19] and (4) ultrasonic cavitation.^[20,21] The strong shearing and high intensity of turbulence in the process can easily break up and disperse fine inclusions and/or fragment dendritic arms, and consequently induce the grain refinement of melt conditioned metals. However, there is hardly any paper showing convincing evidence of heterogeneous nucleation of aluminum grains on the fine particles, because the size and volume fraction of potential particles for the nucleation are too small to analyze in an actual melt conditioned sample.^[22] It is also difficult to detect the fragmented aluminum due to its undistinguishable morphology with aluminum matrix.

For almost 60 years, twin roll casting (TRC) has been used in the aluminum industry to reduce a movement of liquid and/or solid within the casting and consequently to increase productivity.^[23-25] The TRC process, which uses the merit of the high solidification rate, produces thin aluminum sheet of about 1 to 5 mm from the melt.^[25,26] However, its productivity and range of alloys which can be cast are limited.^[24] The lack of surface scalping causes serious defects at the casting stage, or during subsequent handling of twin roll cast reroll stock.^[27] In addition, centerline segregates are inherent to the process. The center region of TRC strips experiences an estimated cooling rate of 100 K/s.^[28] This high cooling rate increases the dendritic growth rate due to the increase of the rate of latent-heat removal,^[23] strongly undercools intermetallic phases in aluminum,^[25] and forms fine structure of eutectic phases,^[13] which causes non-equilibrium solidification

KEEHYUN KIM, Research Fellow, is with the The EPSRC Centre - LiME, School of Metallurgy and Materials, University of Birmingham, Edgbaston, Birmingham B15 2TT, U.K. Contact e-mail: k.kim.2@bham.ac.uk

Manuscript submitted February 13, 2014.

Article published online July 2, 2014

to the TRC process. The build-up of rolling pressure by twin rolls increases the rate of heat extraction, and this also leads to rapid solidification of the trapped liquid which is enriched in solute elements between the rolls.^[24,25] Moreover, the high casting speed promotes to form a deep sump with a large volume of liquid between the fronts of solidifying grains coming from each roll. As a consequence, large amounts of solute atoms are rejected from the liquid and finally form channeling segregation at the strip center.^[13,23,25] The severe centerline segregation results in serious quality problems particularly at foil thickness.^[28] However, it is well known that in pure aluminum, little or no segregation can be observed even at high casting speed.^[25] Therefore, if uniform alloy contents and solidification induced by uniform temperature can be achieved, the centerline segregation is minimized.

Recently, a novel technique using the intensive melt shearing process was used to minimize the centerline segregation as well as to induce the structural uniformity.^[12,13] In the process, enhanced heterogeneous nucleation of aluminum grains on well-dispersed fine oxide particles may minimize or diminish the severe centerline segregation,^[9,11,29–31] although inclusions such as oxides, carbides, and borides are generally detrimental to the mechanical and corrosion properties of cast aluminum strip and promote hydrogen porosity.^[32,33] However, there is little agreement on the heterogeneous nucleation on oxides due to their poor wettability and high contact angles of liquid aluminum and oxides.^[30] Therefore, it is imperative to detect directly any oxides in the sample showing the possibility of the heterogeneous nucleation. In this study, the oxide existing at the center of an aluminum grain in an intensively sheared sample has been investigated to show unequivocal and convincing evidence for the heterogeneous nucleation. Furthermore, high-resolution electron microscopy has been used to reveal the exact macro-/micro-segregations of TRC samples.

II. EXPERIMENTAL

An AA 5754 aluminum alloy with the composition of Al-3.12Mg-0.05Si-0.2Fe-0.43Mn-0.001Cu-0.02Ti (wt pct) was used for TRC or MC-TRC process. The alloy was melted in a clay graphite crucible at 1028 K (755 °C) and poured into a laboratory scale horizontal twin roll caster installed in Brunel University. The roll gap and tundish tip were set at 3 and 43 mm from the center of the gap, respectively. The casting speed was 1 to 2 m/min and the strip thickness was about 5 mm. For MC-TRC, the melt was poured into the MC unit at 953 K (680 °C), melt conditioned at 500 rev/min at 928 K (655 °C) for 60 seconds by twin screws, and then cast by the twin roll caster. The TRC and MC-TRC processes are fully described elsewhere.^[13,14]

The samples were submitted to standard cutting, grinding, and polishing operations. For optical microscopy (OM) and scanning electron microscopy (SEM), the surfaces of TRC and MC-TRC samples were etched by a solution (100 mL distilled water, 4 g potassium

permanganate, 1 g sodium hydroxide). Then, the etched surfaces and non-etched cross-sections, respectively, were observed by OM and SEM. Figure 1 shows the sampling and observation directions performed in this study. Just the top half part of each strip was ground and polished to reveal the morphology of the centerline segregation by high-resolution electron microscopy (Figure 1(d)). For the observation, the strip was cut into the size of 10 × 10 × 5 mm, and then four sides of the cut sample were polished to confirm the centerline segregation at each side and to check the distance to the centerline during the grinding and polishing of the top part. Microstructural observations using SEM were carried out with a field emission gun SEM (JEOL JSM-7000F) equipped with an electron dispersive X-ray spectrometer (EDX) and a focused ion beam (FIB) SEM (FIB-SEM, FEI Quanta 3D) equipped with dual (ion and electron) beam and an EDX system. Three different SEM imaging modes of secondary electron (SE), back-scattered electron (BSE), and ion-induced SE (IS) were used for clear observations of the surface, the centerline segregations, and each grain. For transmission electron microscopy (TEM), thin electron-transmitting specimens were fabricated by a FIB lift-out technique,^[34–36] and then observed by a high-resolution microscope (FE-TEM, FEI Tecnai F20) with a scanning mode (STEM) and an EDX system, and a superior TEM (JEOL JEM-2100FCS) with a spherical aberration (C_s) corrector, as well as a STEM mode and an EDX.

III. RESULTS

A. Macro-segregation of TRC Sample

Figure 2 shows typical OM and SEM images of the surfaces of TRC and MC-TRC samples. In the TRC

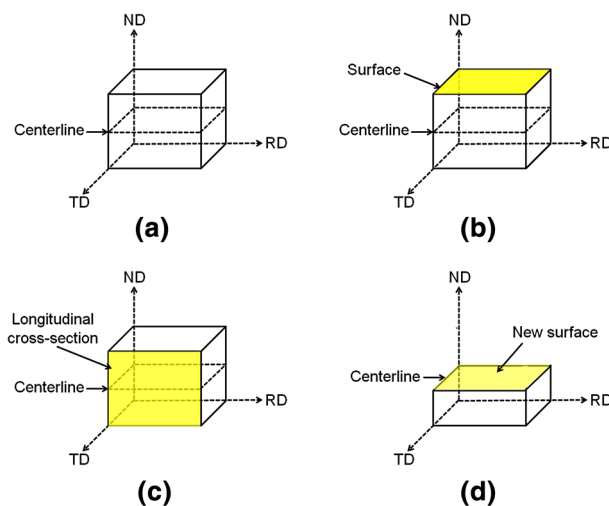


Fig. 1—Directions of sampling and SEM observation: (a) rolling (RD), transverse (TD), and normal (ND) directions, (b) to (d) planes of SEM observations in Figs. 2 and 5, 6, 7, 8, 9(b), Fig. 3(c), and Fig. 4(d).

sample, large different contrast displays through the surface as indicated by arrows. A SEM-BSE image (Figure 2(c)) using Z-contrast clearly shows large amounts of heavier elements, such as iron and manganese, than main aluminum matrix or solute magnesium in the dark contrast region of Figure 2(a). By contrast, the melt conditioned TRC sample shows uniform distribution of the heavy elements through the surface (Figures 2(b) and (d)).

It is well known that the combined solidification and rolling process forms channels with almost constant spacing in the central plane of TRC sheet.^[24–27] As a result, as shown in Figure 3(a), large amounts of inclusions are segregated along the centerline, which is the so-called centerline segregation. However, it is clear that the melt conditioning minimizes the centerline segregation (Figure 3(b)).

In order to understand the segregation, high-resolution SEM which is available to the range of magnification of 25,000 \times to 50,000 \times was used at a working distance of about 10 mm (Figure 4). Figure 4(a) is a typical morphology of the centerline segregation composed of diverse Al-Fe-Mn phases.^[33,37] In Figure 4(b), there are tenfold star-like $\text{Al}_{13}\text{Fe}_4$ particles which formed by a multiple twinning mechanism in a high iron containing aluminum alloy.^[13,38] Specifically, two types of Mg_2Si phase are detected: one is the discrete

polygonal-shaped Mg_2Si (black particles in Figure 4(c)), the other typical eutectic Mg_2Si (Figure 4(d)).

B. Micro-segregation of MC-TRC Sample

Melt conditioning of the TRC sample clearly minimizes the centerline segregation as shown in Figure 3. However, as the same raw materials (AA5754) including magnesium, silicon, iron, and manganese were used for the TRC and MC-TRC samplings in this study, it is imperative to investigate the distribution of the solute elements in MC-TRC samples because they must exist within the samples.

For comparison, the surface of TRC sample was observed by high-resolution SEM before observing the MC-TRC sample. As already shown in Figure 2, solute elements form macro-segregation on the surface. Figure 5 is high-magnification SEM images and SEM-EDX element maps of main solute elements near grain boundaries. It is clear that magnesium, silicon, and iron are severely segregated along the boundaries. Particularly, an intact dendrite mainly composed of aluminum and iron is clearly observed (Figure 5(e)). Eutectic Mg_2Si is also visible even if the surface is damaged by the preferential attack of the etching solution (Figure 5(f)).

Figure 6 shows SEM images and SEM-EDX point analyses of the surface of MC-TRC sample. In order to

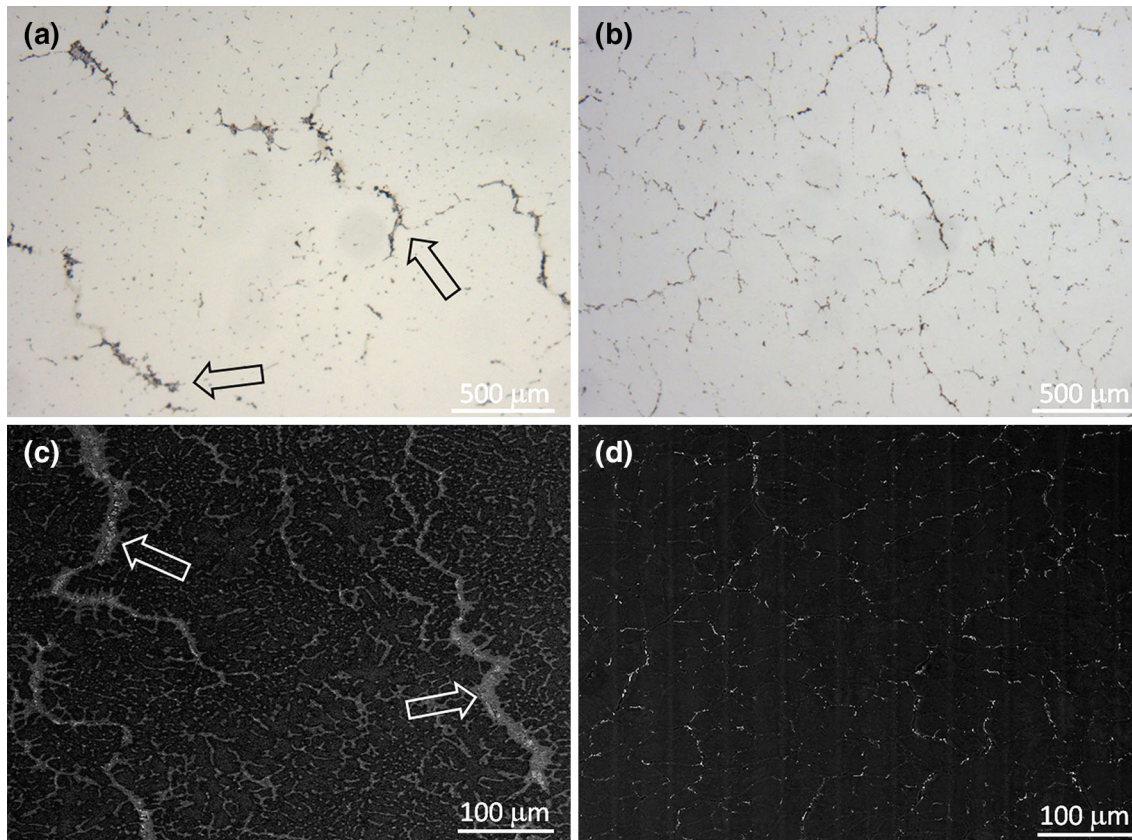


Fig. 2—Surface observations of TRC (a), (c) and MC-TRC (b), (d) samples: (a), (b) optical microscopy, and (c), (d) SEM-BSE images. The arrows in panels (a) and (c) indicate macro-segregation.

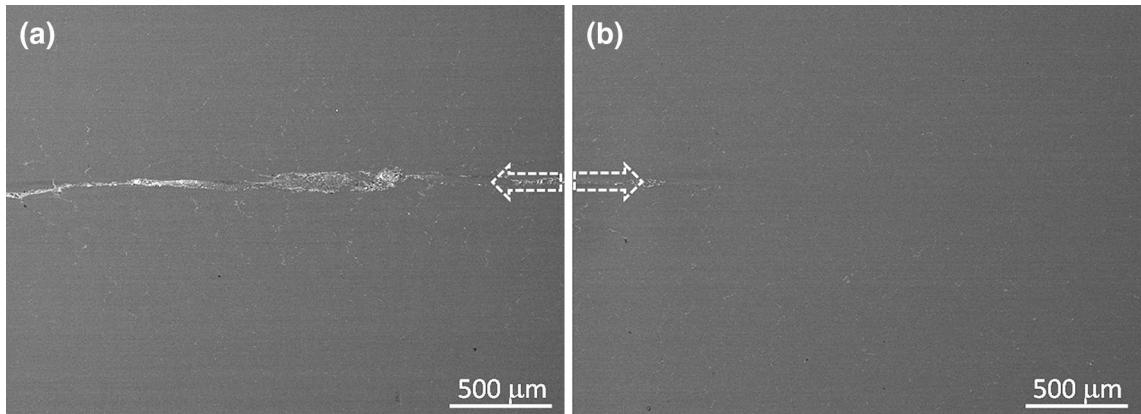


Fig. 3—SEM-BSE images near the centerlines of TRC (a) and MC-TRC (b) samples. The arrows indicate the centerline of each sample.

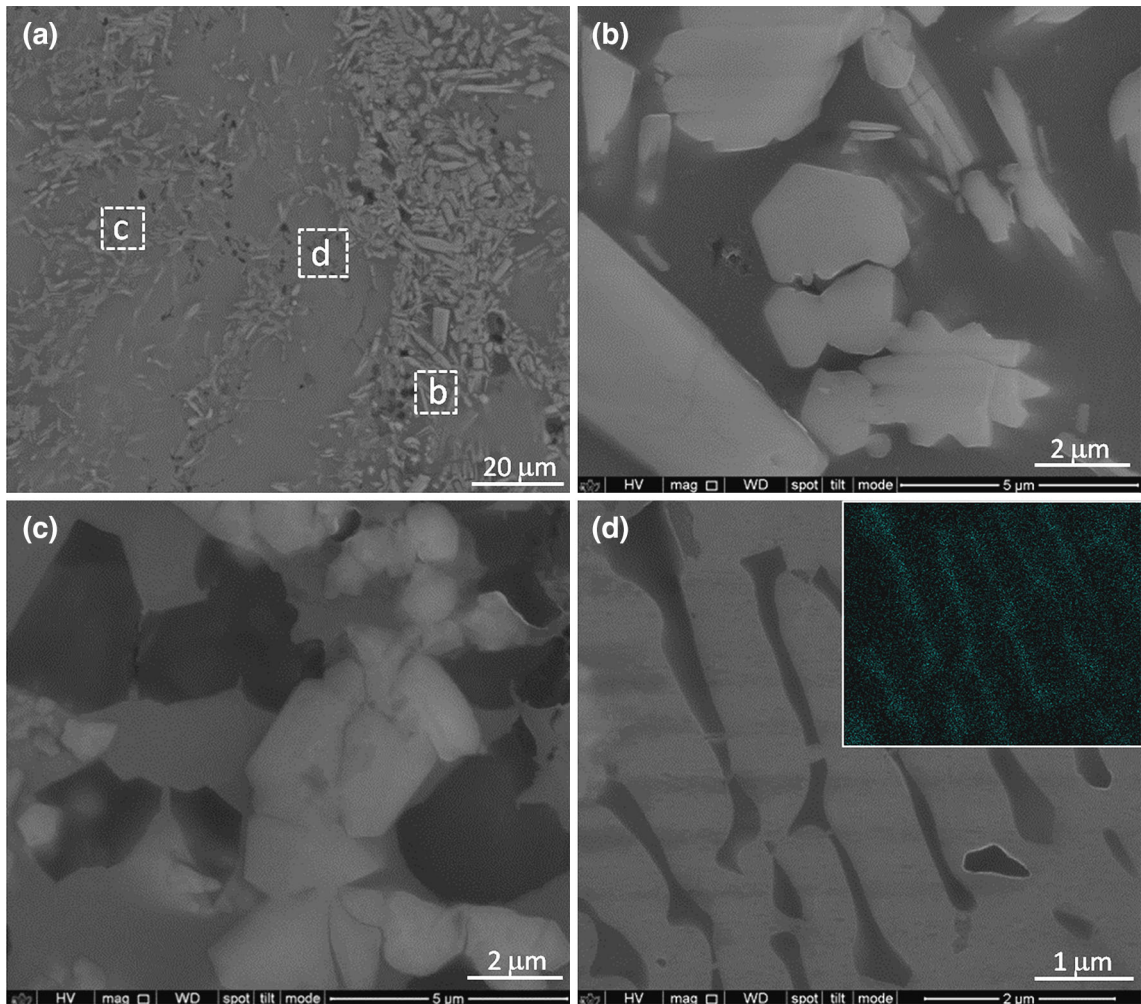


Fig. 4—SEM images of centerline segregation of TRC sample: (a) typical image of segregated particles, (b) to (d) magnified images of the marked regions in panel (a). The inset in (d) is the corresponding SEM-EDX element map of silicon.

observe exactly the sample region by SEM-SE and SEM-IS, a plus (+) was intentionally marked by FIB milling at the top of the observed area (Figure 6(a)). The solute elements are uniformly distributed through the surface, especially, along the boundaries (see also

Figure 7). A high-magnification SEM-SE image (Figure 6(b)) clearly shows that there are numerous fine particles mostly composed of aluminum and iron at the boundaries, even though the size of particles is too small to analyze obviously by SEM-EDX due to the inherent size

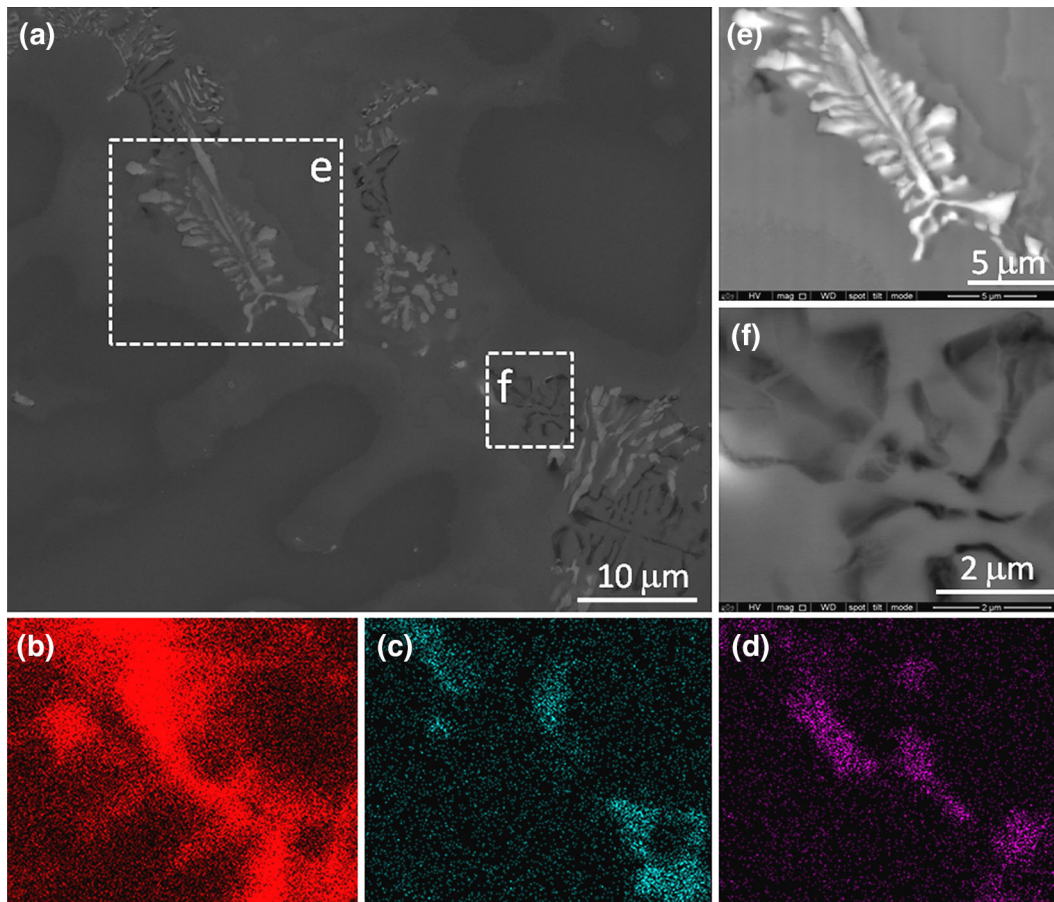


Fig. 5—SEM analysis of micro-segregation of the surface of TRC sample: (a) SEM-SE image, (b) to (d) corresponding SEM-EDX element maps of magnesium (b), silicon (c), and iron (d), and (e), (f) magnified SEM-BSE images of the marked regions in panel (a), respectively.

limitation of SEM-EDX microanalysis.^[39] In another region (Figure 6(c)), however, there are larger particles along the boundaries, which are available for the point analysis by SEM-EDX. The matrix (grain) is nearly pure aluminum (Figure 6(d)). Large amounts of magnesium (Figure 6(e)) as well as some broken iron-rich phases (Figure 6(f)) exist along the boundaries. First of all, some oxides are clearly detected (Figure 6(g)). Although it has been suggested the possibility of heterogeneous nucleation of aluminum grains on fine particles including oxides, there is little to no convincing evidence of the existence of any oxide in an actual melt conditioned sample. Hence, the detected oxide particles along grain boundaries deserve careful consideration, which is discussed further later. It should be noted that the size of each particle in the MC-TRC sample is much finer than the particle size in the TRC sample, while the TRC and MC-TRC samples show similar grain morphology and slightly different grains sizes of about 10 pct.

C. Nucleation of Aluminum Grains

Figure 7 is SEM images and SEM-EDX element maps near a grain including a fine particle at the center. Even though it is difficult to distinguish a fine particle in SEM-SE (Figure 7(b)), SEM-EDX element maps of aluminum

(Figure 7(c)) and magnesium (Figure 7(d)) shows clearly the existence of a different particle. Additionally, there are other two grains including a fine particle at the center of each grain marked with arrows in Figure 7(a). Figures 7(e) and (f) are the maps of iron and silicon, respectively. As main solute elements of magnesium, silicon, and iron in an AA5754 alloy have a negative slope of the liquidus line and a partition coefficient of below 1,^[23,40] their solubilities are larger in the liquid aluminum than in the solid. Consequently, they are rejected from the front of the growing grains, and finally enriched in grain boundaries where the liquid completes solidification. It is worth noting that only one particle is detected exactly at the center of one grain and first of all, other solute elements and particles are not detected within the grain, which is meaningful to distinguish the nucleant with the engulfed particle (see the next section).

A FIB lift-out technique was used to make exquisitely a TEM sample on a particle detected at the center of one grain. A grain was selected and marked intentionally with two distinguishable 'X's during sampling (Figure 8(a)). Prior to the marking, the existence of a magnesium-rich particle as shown in Figure 7 was confirmed by SEM-EDX. A thin tungsten layer was deposited on the particle and then trenches were made near the particle (Figure 8(b)). FIB milling gradually

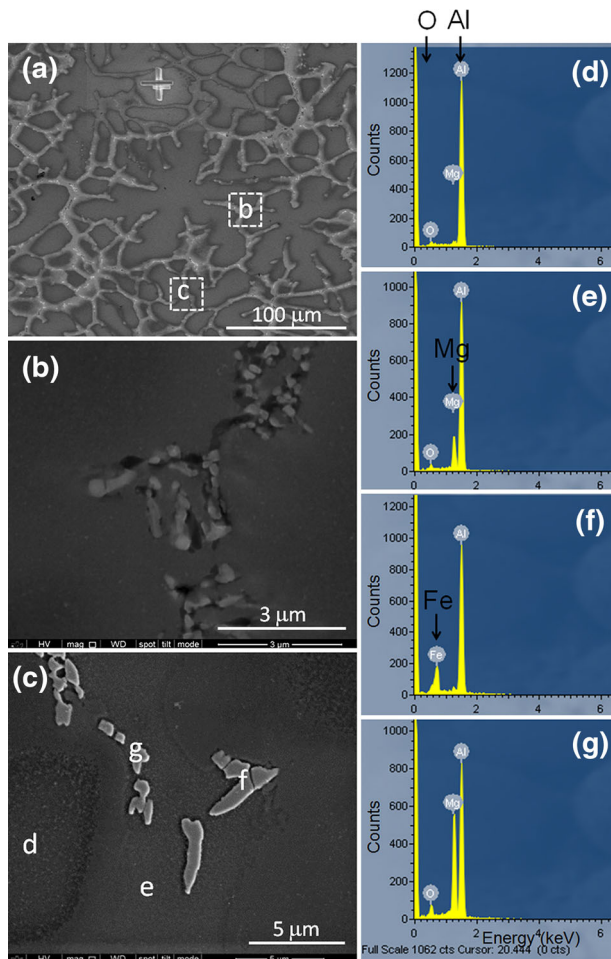


Fig. 6—SEM analysis of micro-segregation of MC-TRC sample: (a) typical image of the surface of MC-TRC sample, (b), (c) magnified images in panel (a), and (d) to (g) SEM-EDX point analysis of the marked points in (c), respectively.

made the region near the particle thinner, and cut left and bottom parts (Figure 8(c)). A micro manipulator lifted out the lamella (Figure 8(d)) and then put it on a copper grid. After final milling and cleaning, a sample thin enough for TEM analysis was made. Figure 8(e) is a TEM-BF image of the particle in Figure 8(a). There is no pore or void near the particle. A STEM-EDX point analysis on the particle clearly indicates that it is composed of magnesium and oxygen (Figure 8(f)). Considering the size of fine oxides existed along the grain boundary, it was concluded that magnesium oxides were distributed not merely at each center of aluminum grains, but also along grain boundaries. However, it should be noted that large oxide particles of about 1 to 5 μm existed at the center of each aluminum grain, whereas small oxides with the size of about 100 to 200 nm were detected only at the grain boundaries. Also, regardless of its size, no oxide was detected within dendritic arms and around grain boundaries.

A previous study using a FIB serial milling and lift-out technique shows a possibility that even though there is no particle exposed on the surface, a particle may exist beneath the surface.^[41] The FIB lift-out technique was

accordingly used to find any other particle at the center region of one grain. Figure 9 shows another interesting finding of two different grains existing near the center. A single grain was selected and marked with two 'X's (Figure 9(a)) and sampled by the FIB technique. Figure 9(b) shows a TEM image and a selected area diffraction pattern of the *grain N* with the zone axis of (102). Figure 9(c) is a STEM-EDX point analysis on the *grain F*. The grain is nearly pure aluminum. After tilting along *x*-axis 3.5 deg and *y*-axis 1.5 deg, the *grain F* has the zone axis of (212) (Figure 9(d)). Moreover, the TEM-DF image using the (202) spot shows that the *grain N* and the *grain F* are two different grains. Furthermore, in the boundary of the two grains, any pore or void as well as alloying elements were not detected. The TEM analysis means that the *grain N* was nucleated on the fragmented *grain F*, which are further discussed later.

IV. DISCUSSION

A. Detection of a Fine Oxide at the Grain Center

The TEM analysis (Figure 8) has shown clearly that a MgO particle can act as a substrate for heterogeneous nucleation of an aluminum grains. However, when the front of a solidifying grain meets dispersed particles, advancing solidification can push the particles into grain boundaries or interdendritic regions, or engulf them into the inside. In addition, there is another possibility of entrapping fine particles (with different thermal conductivities) into the solidifying grains, which is suggested in References 42 and 43. Hot particles in front of the tips of solidifying grains can keep the surrounding liquid at high temperature, split the solidifying grains or dendritic arms, and then remain inside the grains during cooling down. In consequence, it has been considered that only the microscopic observation of particles inside grains may not be unequivocal and convincing evidence of the heterogeneous nucleation of grains on the particles, although the observation of fine particles inside grains has been used as the evidence of the heterogeneous nucleation.^[4,44–52] Furthermore, it is well known that crystallographic orientation relationship between nucleating grains and particles should exist for the effective nucleation. Recently, however, Schaffer *et al.*^[53] have highlighted from extensive TEM analysis of the orientation relationship over 50 particles that even engulfed particles display well-defined orientation relationships with the matrix. Thus, showing the relationship itself may not be evidence of the heterogeneous nucleation. Considering literature which reported the engulfment of particles, it is interesting to find that there are differences between the engulfed and the nucleant particles. In the engulfed case, several particles were engulfed by a solidifying grain.^[42, 53] Consequently, they were detected within 'one' grain, then distributed through the grain, not only near the center region.^[42,53] Furthermore, even if the particles are engulfed accidentally into the center region from each dendritic arm, a cluster composed of several fine particles must be detected. Most of all, there should be pore or void near the entrapped particle(s) due to the different thermal conductivities with the

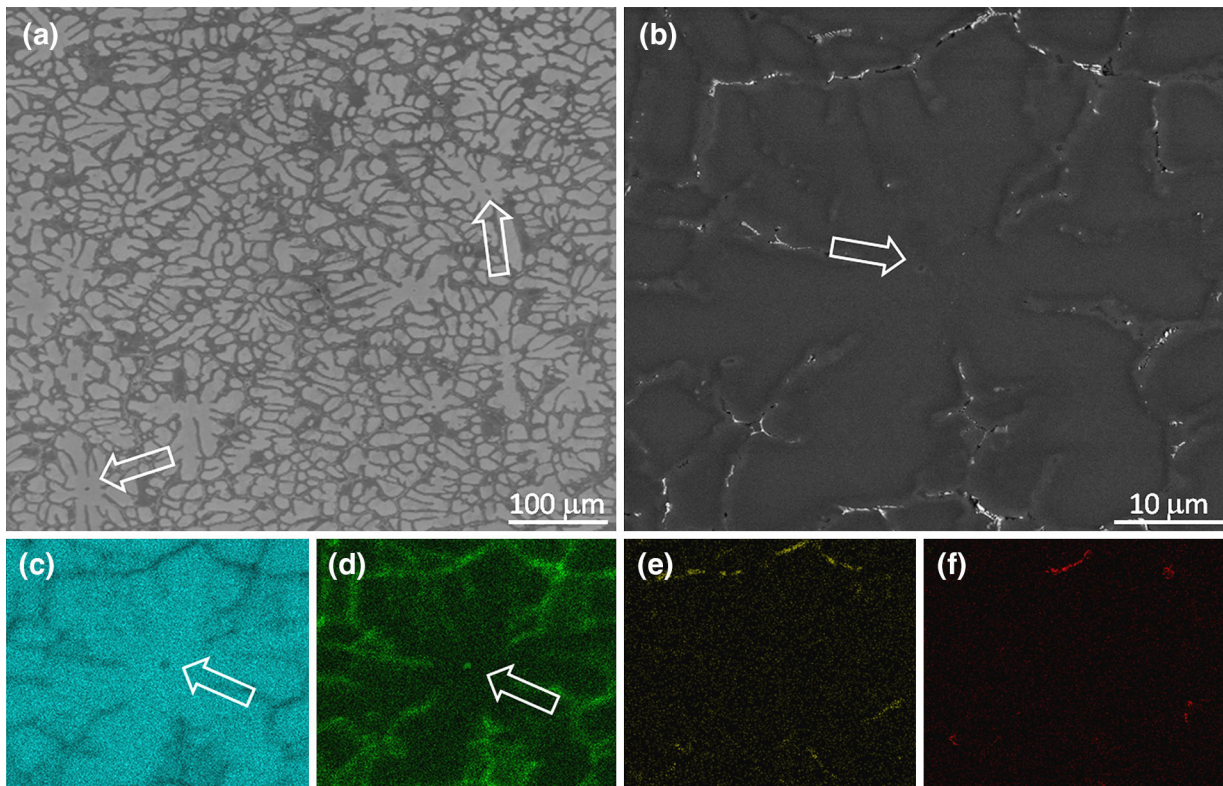


Fig. 7—SEM analysis a fine particle detected at the center of an aluminum grain: (a) typical image showing the fine particles located at the center of each grain, and (b) to (f) SEM-SE image of a grain (b) and corresponding SEM-EDX element maps of aluminum (c), magnesium (d), iron (e), and silicon (f). The arrows indicate the particles located at the center of each grain.

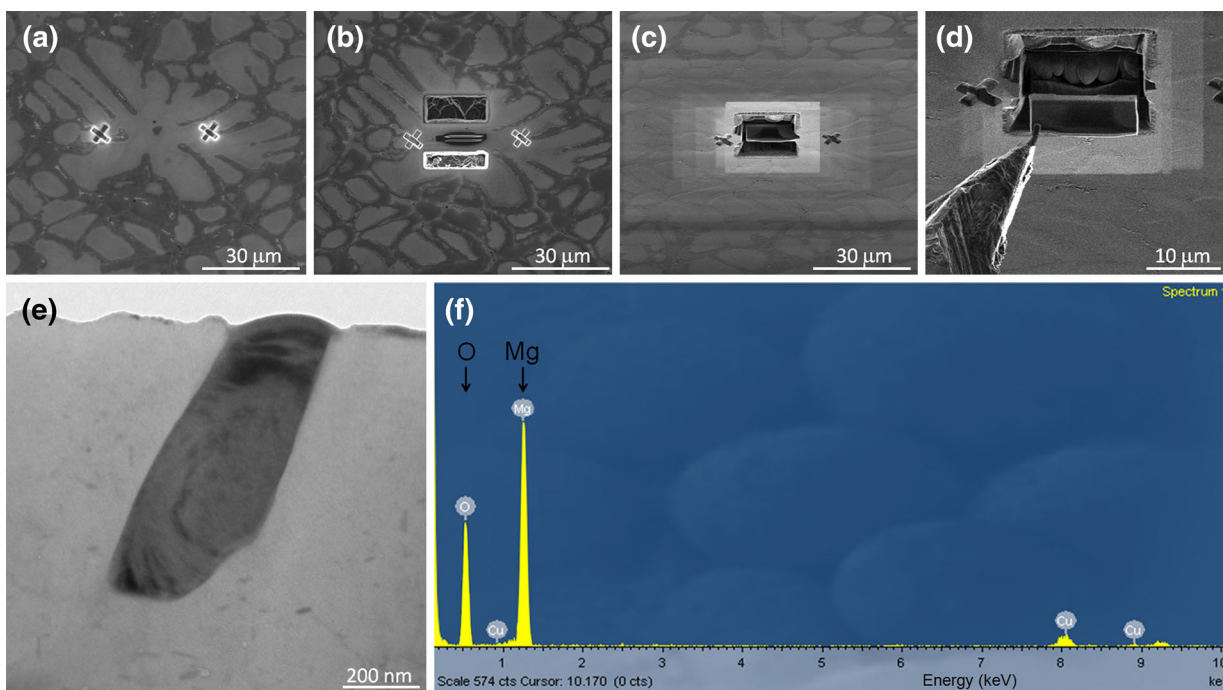


Fig. 8—TEM sampling (a) to (d) and analysis (e), (f) of a fine particle located at the center of an aluminum grain: (a) selected grain with two 'X' s marked intentionally by FIB milling, (b) protective tungsten deposition and milling near the center region in panel (a), (c) before lifting out the lamellae, (d) lifting out with a micro manipulator, and (e), (f) TEM-BF image (e) and TEM-EDX point analysis (f) of the particle. Note that x-axis in the TEM-EDX spectrum indicates 'Counts'.

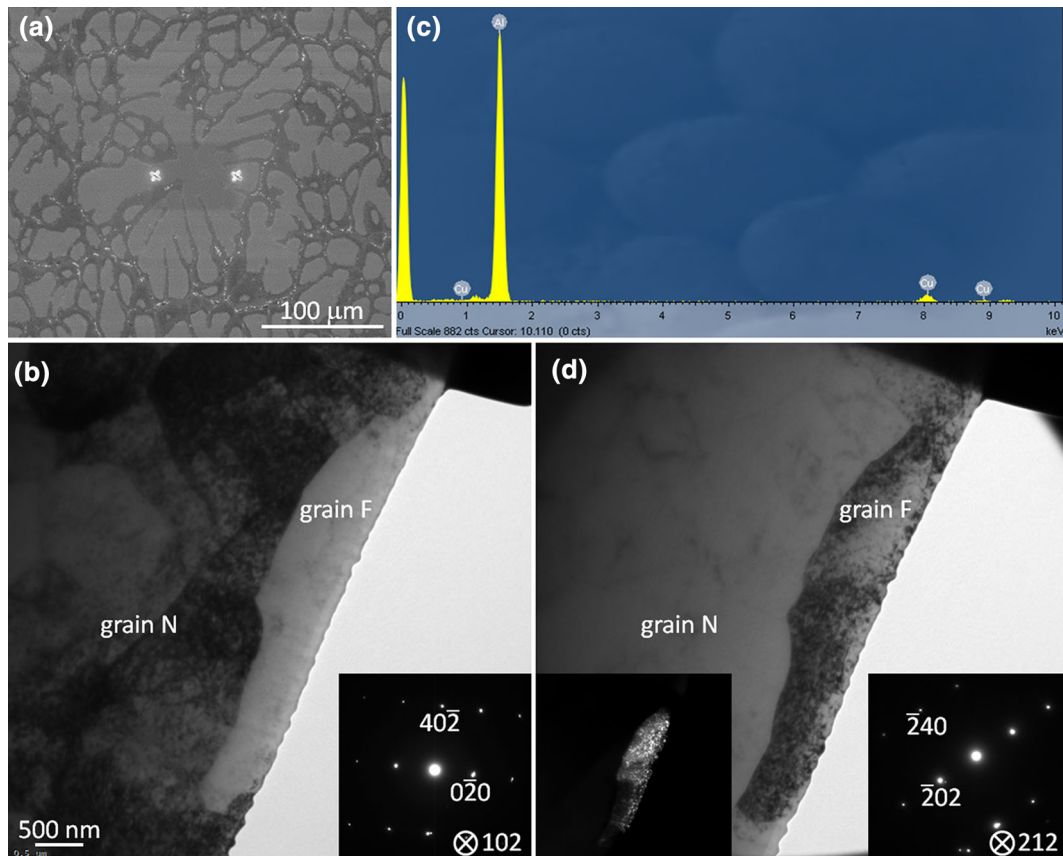


Fig. 9—TEM analysis of the center of an aluminum grain: (a) selected grain with two ‘X’s marked intentionally by FIB milling, (b) TEM-BF image near the center region with a SADP of *grain N*, (c) TEM-EDX point analysis of *grain F*, and (d) TEM-BF and corresponding TEM-DF (inserted) images after tilting of *x*-axis about 3.5 deg and *y*-axis 1.5 deg at the position of panel (b) with a SADP of *grain F*.

matrix metal.^[42,43] Conversely, if the particles act as substrates for the heterogeneous nucleation of matrix grains, only one particle will exist in each grain, especially near the center region.^[4,44–52] In addition, since the particle acted as the substrate for the nucleation, there must not be any pore or void near the particle due to intimate bonding or interaction between the nucleated grain and the particle. Hence, only one MgO particle which was detected exactly at the center of an aluminum grain without any other particles (Figure 8) is unequivocal and convincing evidence for the heterogeneous nucleation. The detection of a particle at the center of a grain in this study is in good agreement with a previous finding of MgO particles acted as the substrate for the heterogeneous nucleation of aluminum grains revealed by a novel technique of FIB serial milling combined with FIB lift-out.^[22]

B. Formation of MgO Acting as the Substrate for Nucleation of Aluminum

Figures 6 and 8 show that MgO not MgAl₂O₄ (spinel) can act as the substrate for the heterogeneous nucleation of aluminum grains. As magnesium has lower surface tension at the melting point of aluminum and higher reactivity than aluminum, the preferential segregation

and oxidation of magnesium happen at the surface of aluminum melt at higher temperatures and consequently, compared to MgAl₂O₄, MgO forms more easily.^[54,55] However, the following reactions based on thermodynamic considerations are suggested for the formation of MgAl₂O₄ on the surface of the liquid metal or at the interface of oxide/melt depending on concentrations of magnesium and aluminum at the reaction sites:^[54,56] $\text{Mg}_{(l)} + 2\text{Al}_{(l)} + 2\text{O}_{2(g)} = \text{MgAl}_2\text{O}_{4(s)}$, and $2\text{MgO}_{(s)} + 4\text{Al}_{(l)} + 3\text{O}_{2(g)} = 2\text{MgAl}_2\text{O}_{4(s)}$. In addition, under normal melting conditions, MgO forms at the initial oxidation stage and consecutively transforms into MgAl₂O₄. It was therefore suggested that the stable oxide with high potency for the heterogeneous nucleation of aluminum grains might have been MgAl₂O₄ rather than MgO.^[29,55] However, in this study, it can be confirmed that the particle which acted as the substrate for heterogeneous nucleation of an aluminum grain can be magnesium oxide. A recent study using Al-4 pct Mg also shows that a porous MgO layer with the thickness of about 5 μm forms at short oxidation time of 5 minutes and then the thickness gradually increases to about 7 μm for 1 hour.^[57] Thereafter, MgAl₂O₄ can be formed by the aforementioned reaction of $2\text{MgO}_{(s)} + 4\text{Al}_{(l)} + 3\text{O}_{2(g)}$. Additionally, it is interesting that X-ray diffraction (XRD) patterns of an Al-10 pct Mg alloy

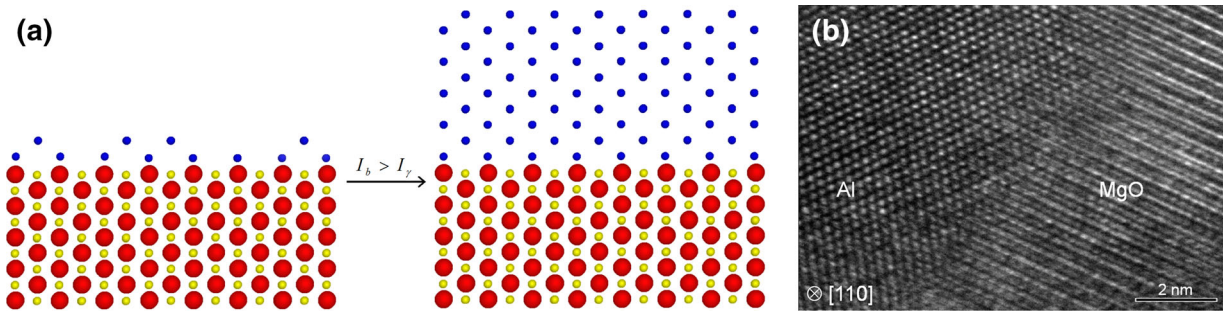


Fig. 10—Schematic diagrams of heterogeneous nucleation of aluminum (a) and representative high-resolution lattice image near the MgO detected in Fig. 8(b). Blue sphere is aluminum, yellow is magnesium, and red indicates oxygen.

oxidized for 3 hours show peaks corresponding to MgO.^[56] McLeod and Gabryel^[58] have presented a thermodynamic stability diagram of Al-Mg oxides including MgO and MgAl₂O₄ in liquid Al-Mg alloys in which they used the free energy of formation and activity coefficient data based on the reaction of magnesium and aluminum oxide. In the diagram, MgO is more stable than MgAl₂O₄ for high magnesium concentrations of above 1.5 pct at 1028 K (755 °C). Thus, even though all MgO existing on the surface of alloy melt were consumed by the reaction of MgAl₂O₄ formation, the aluminum melt containing magnesium can rise into capillary MgAl₂O₄ tubes because MgAl₂O₄ exists in the melt as discrete particles due to low Pilling–Bedworth ratio.^[55] In consequence, the melt can reoxidize repeatedly to form MgO and survive during melting and intensively melt shearing, which means that MgO can survive and act as the substrate for the heterogeneous nucleation of aluminum grains during solidification.

C. Nucleation Mechanism of Aluminum Grains on Oxide Particles

On comparing the size of oxide particles detected in grain boundaries (Figure 6(c)) with that of the nucleant oxide particle at the center of an aluminum grain (Figure 8), it is interesting to find that there is a size dependence of nucleation potency of oxide particles. Greer *et al.*^[8] have developed a free growth model to suggest that nucleation of an aluminum grain starts and grows free on a nucleant particle at an undercooling. The relation of the undercooling (ΔT_g) necessary for the free growth of aluminum through the minimum-radius hemispherical shape with the diameter (d) of nucleant particles is expressed as the following:^[8,31]

$$\Delta T_g = \frac{4\gamma_{sl}}{\Delta S_f \cdot d},$$

where γ_{sl} is the interface energy of solid/liquid and ΔS_f the fusion entropy per unit volume. It is clear that the undercooling for the free growth is inversely proportional to the diameter of particles. Therefore, small oxides with the size of about 100 to 200 nm requiring large undercooling could not nucleate heterogeneously aluminum grains and consequently they were pushed

into the grain boundaries (Figure 6). By comparison, large oxide particles of about 1 to 5 μm could nucleate easily aluminum grains due to the low undercooling necessary for the heterogeneous nucleation (Figure 8).

There is a question about the heterogeneous nucleation of aluminum grains on MgO particles: what is the mechanism of the nucleation? Oh *et al.*^[59] have observed clearly an interesting phenomenon at the interface of solid/liquid. Real-time high temperature observation shows the ordering of liquid atoms adjacent to an interface with a crystal at the atomic-length scale, especially, at the interface of solid alumina and liquid aluminum. Likewise, two atomic layers of metallic atoms on the surface of ceramic substrate form an epitaxial and coherent heterointerface due to the preferential attachment of metallic atoms to specific sites on the surface of the substrate.^[60] In addition, the electron density of oxygen atoms at the top-layer of MgO induces strong bonds to the interface of oxygen-terminated MgO and aluminum by the ionic component and covalent/metallic contribution.^[61] Based on these explanations of the initial attachment of metallic atoms on oxides, a schematic diagram of Figure 10(a) indicates the heterogeneous nucleation of an aluminum grain on the particle of MgO. Aluminum atoms in liquid are ordered by the strong bonding between aluminum and oxygen of the top-layer of MgO. It means that the surface of MgO particle is covered with aluminum atoms in liquid, which is important to induce the heterogeneous nucleation. It is noted that if solute magnesium atoms in melt exist at the interface of Al/MgO, they can be also ordered due to their high affinity to oxygen. However, as the thickness of the ordered aluminum layer increases or the solidification of the melt commences, the effect of interface energy increases. If the intensity of interface energy (I_γ) exceeds that of bonding energy (I_b), *i.e.*, if $I_\gamma > I_b$, the aluminum atoms detach from the substrate. In contrast, if $I_\gamma < I_b$, the atoms survive and grow continuously. Figure 10(b) is a high-resolution lattice image acquired at the interface of MgO/aluminum of Figure 8, and demonstrates the heterogeneous nucleation of aluminum on MgO (110). Similarly, an epitaxial model is recently suggested to explain heterogeneous nucleation on potent substrates.^[62] Atomic-level epitaxial growth of a pseudomorphic layer takes place, beyond a critical

undercooling, on a potent substrate. However, since the model is based on the creating of misfit dislocations at the interface of pseudomorphic layer/substrate, a good lattice mismatch is an essential prerequisite, which is different from this study based on the ordering of liquid elements by the strong bonding across the interface. In any case, it is clear that the interface energy is significantly affected by many factors, such as grain size, crystal structure, misfit dislocations in the interface of substrate/nucleated metal, lattice mismatch, orientation relationship, chemical nature and electrostatic potential between them.^[63–65] However, if any nucleation occurs on the same material, the interface energy minimizes and consequently the nucleation can occur easily.^[5]

The TEM analysis (Figure 9) at the center of a single aluminum grain suggested its nucleation on a fragmented aluminum grain. It is well known that the fragmented grains have an effect on the microstructural change. Moreover, they can induce the grain refinement in undercooled melts.^[66,67] There are two possibilities of the fragmentation of aluminum grains: one is that in the mushy zone, the high pressure of twin rolls can fragment primary grains and then other aluminum grains are nucleated on the fragmented ones, and the other is that the fragmentation occurs during intensive shearing, remains in the melt, and finally nucleates other aluminum grains. If the fragmentation occurs in the mushy zone, it must be detected inside the MC-TRC sample because solidification commences from the surface into the center and the high pressure of twin rolls pushes them into the center region. However, it was on the surface of MC-TRC sample that the fragmented aluminum grain was detected in Figure 9. In other words, the fragmented grain was observed at the surface where solidification had commenced. Therefore, it was concluded that the fragmented grain had already existed in the melt and nucleated an aluminum grain.

D. Effect of Intensive Shearing on Segregation of Solute Atoms

In TRC process, two opposite growing interfaces of solidified/liquid aluminum from twin rolls partition solute elements into the center region, and at the last stage of solidification the center region of cast strip including large amounts of solute atoms are solidified.^[13,26,28] After the solidification, several kinds of intermetallic compounds, such as Mg_2Si and $Al_{13}(Fe, Mn)_4$, form at the center. However, in MC-TRC process, intensive shearing breaks up oxide particles and disperses them through the liquid. As a consequence, the intensive shearing of aluminum melt increases the number density of active particles for the heterogeneous nucleation of aluminum grains as much as about a factor of 20.^[31] The dispersed oxides can help or act as nucleant substrates for intermetallics or aluminum. In addition, the intensive shearing evenly distributes the solute atoms through the melt. The enhanced nucleation of aluminum grains and well-distributed solute atoms form a uniform microstructure

of aluminum grains surrounded with solute atoms. Therefore, the centerline segregation is minimized because most of solute atoms have been already exhausted before the hot deformation or channeling. Furthermore, the fragmented aluminum grains can also contribute to the nucleation of other aluminum grains and distribute more solute elements along the grain boundaries or interdendritic regions.

V. CONCLUSIONS

It has been suggested that, in melt conditioning processes, heterogeneous nucleation of aluminum or magnesium grains on fine and well-dispersed oxide particles may induce the grain refinement and structural uniformity. This study clearly shows that oxides, which have been generally considered detrimental to mechanical properties and corrosion resistance, can act as substrates for the nucleation of aluminum grains. However, depending on the size of oxide particles, there are different efficiencies of nucleation potency. Small particles requiring large undercooling for the free growth of nucleating grains are pushed into grain boundaries by the solidification front, whereas large particles nucleate aluminum grains relatively easily due to the low undercooling. During the intensive shearing of melt, MgO is easily broken up and well dispersed by the high shear rate and high intensity of turbulence, and nucleates heterogeneously aluminum grains. Fragmented aluminum grains also contribute to the nucleation of other aluminum in the melt conditioned sample. These intense nucleations in the intensively sheared melt minimize the severe centerline and surface segregations. The intensive shearing also distributes uniformly other phases, such as iron-rich phases and Mg_2Si , along grain boundaries, which *probably* improve high temperature and mechanical properties of the intensively sheared aluminum.

Finally, it should be noted that a fragmented aluminum grain which acted as the substrate for another aluminum grain was detected and observed (Figure 9). However, the survival of the fragmented grain during the intensive shearing carried out at 928 K (655 °C) for 60 seconds or in aluminum melt remains as a matter to be discussed further.

ACKNOWLEDGMENTS

The author thanks Dr. W. D. Griffiths and Prof. N. R. Green of University of Birmingham for financial support under EPSRC Grant EP/H026177/1, Prof. Z. Fan of Brunel University, Dr. S. Kumar of Oxford University, and Mr. A. Powell of University of Birmingham for supplying the material for investigation, Mr. R. Hibberson and Mr. A. Scarratt of Struers Ltd., for the metallographic sample preparation, particularly Prof. Jian-Feng Nie and his review committee for the constructive comments.

REFERENCES

1. Y. Kimura, T. Inoue, F. Yin, and K. Tsuzaki: *Science*, 2008, vol. 320, pp. 1057–60.
2. D. StJohn, M. Qian, M. Easton, P. Cao, and Z. Hildebrand: *Metall. Mater. Trans. A*, 2005, vol. 36A, pp. 1669–79.
3. Y. Zhang, N. Ma, H. Yi, S. Li, and H. Wang: *Mater. Des.*, 2006, vol. 27, pp. 794–98.
4. F. Wang, Z. Liu, D. Qiu, J.A. Taylor, M.A. Easton, and M.-X. Zhang: *Acta Mater.*, 2013, vol. 61, pp. 360–70.
5. J.A. Dantzig and M. Rappaz: *Solidification*, CRC Press, Lausanne, 2009.
6. N. Iqbal, N.H. van Dijk, S.E. Offerman, M.P. Moret, L. Katgerman, and G.J. Kearley: *J. Non-Cryst. Solids*, 2007, vol. 353, pp. 3640–43.
7. A. Cibula: *J. Inst. Met.*, 1949, vol. 76, pp. 321–60.
8. A.L. Greer, A.M. Bunn, A. Tronche, P.V. Evans, and D.J. Bristow: *Acta Mater.*, 2000, vol. 48, pp. 2823–35.
9. Y. Zuo, H. Li, M. Xia, B. Jiang, G.M. Scamans, and Z. Fan: *Scripta Mater.*, 2011, vol. 64, pp. 209–12.
10. P. Shen, H. Fujii, T. Matsumoto, and K. Nogi: *Acta Mater.*, 2004, vol. 52, pp. 887–98.
11. Z. Fan, Y. Wang, M. Xia, and S. Arumuganathar: *Acta Mater.*, 2009, vol. 57, pp. 4891–4901.
12. I. Bayandorian, Y. Huang, Z. Fan, S. Pawar, X. Zhou, and G.E. Thompson: *Metall. Mater. Trans. A*, 2012, vol. 43A, pp. 1035–47.
13. S. Kumar, N. Hari Babu, G.M. Scamans, and Z. Fan: *Mater. Sci. Technol.*, 2011, vol. 27, pp. 1833–39.
14. Z. Fan, M.J. Bevis, and S. Ji: US 6745818B1, 1999.
15. S. Jones, A.K.P. Rao, and Z. Fan: *Trans. Indian Inst. Met.*, 2013, vol. 66, pp. 117–21.
16. Z. Fan, B. Jiang, and Y. Zuo: WO2012035357, 2013.
17. W. Braunbek: *Z. Physik*, 1932, vol. 73, pp. 312–34.
18. V. Metan and K. Eigenfeld: *Eur. Phys. J. Spec. Top.*, 2013, vol. 220, pp. 139–50.
19. C. Vives and C. Perry: *Int. J. Heat Mass Transf.*, 1986, vol. 29, pp. 21–33.
20. G.I. Eskin: *Ultrason. Sonochem.*, 1994, vol. 1, pp. S59–S63.
21. G.I. Eskin: *Ultrason. Sonochem.*, 2001, vol. 8, pp. 319–25.
22. K. Kim: *Mater. Lett.*, 2014, vol. 117, pp. 74–77.
23. A.K. Dahle and L. Arnberg: *JOM-J. Miner. Met. Mater. Soc.*, 1996, vol. 48, pp. 34–37.
24. M. Yun, S. Lokyer, and J.D. Hunt: *Mater. Sci. Eng. A*, 2000, vol. 280, pp. 116–23.
25. I. Jin, L.R. Morris, and J.D. Hunt: *J. Met.*, 1982, vol. 34, pp. 70–4.
26. C. Gras, M. Meredith, and J.D. Hunt: *J. Mater. Process. Technol.*, 2005, vol. 167, pp. 62–72.
27. H. Westengen and K. Nes: *J. Met.*, 1983, vol. 35, p. 76.
28. Y. Birol: *Aluminium*, 1998, vol. 74, pp. 318–21.
29. Y. Wang, H.T. Li, and Z.Y. Fan: *Trans. Indian Inst. Met.*, 2012, vol. 65, pp. 653–61.
30. R. Haghayeghi, E.J. Zoqui, and H. Bahai: *J. Alloys Compd.*, 2009, vol. 481, pp. 358–64.
31. H. Men, B. Jiang, and Z. Fan: *Acta Mater.*, 2010, vol. 58, pp. 6526–34.
32. Y. Birol: *Int. J. Cast Met. Res.*, 2010, vol. 23, pp. 250–55.
33. A. Tewari, S. Vijayalakshmi, S. Tiwari, P. Biswas, S. Kim, R. Mishra, R. Kubic, and A. Sachdev: *Metall. Mater. Trans. A*, 2013, vol. 44A, pp. 2382–98.
34. K. Kim, M. Watanabe, K. Mitsuishi, K. Iakoubovskii, and S. Kuroda: *J. Phys. D Appl. Phys.*, 2009, vol. 42, p. 065304 (5 pp).
35. K. Kim, S. Kuroda, and M. Watanabe: *J. Therm. Spray Technol.*, 2010, vol. 19, pp. 1244–54.
36. K. Kim, M. Watanabe, S. Kuroda, and N. Kawano: *Mater. Trans.*, 2011, vol. 52, pp. 439–46.
37. C.M. Allen, K.A.Q. O'Reilly, B. Cantor, and P.V. Evans: *Prog. Mater. Sci.*, 1998, vol. 43, pp. 89–170.
38. D.H. Kim: *J. Korean Inst. Met. Mater.*, 1994, vol. 32, pp. 64–73.
39. D. Brandon and W.D. Kaplan: *Microstructural Characterization of Materials*, Wiley, Chichester, 2008.
40. L.F. Mondolfo: *Aluminium Alloys: Structure and Properties*, Butterworths, London, 1976.
41. K. Kim, N. Green, and W. Griffiths: *Mater. Sci. Forum*, 2013, vol. 765, pp. 150–54.
42. A.E. Karantzalis, A. Lekatou, E. Georgatis, T. Tsiliogiannis, and H. Mavros: *J. Mater. Eng. Perform.*, 2010, vol. 19, pp. 1268–75.
43. W. Zhou and Z.M. Xu: *J. Mater. Proc. Technol.*, 1997, vol. 63, pp. 358–63.
44. S. Erik Naess and J.-A. Rønningen: *Metallography*, 1975, vol. 8, pp. 391–400.
45. J.G. Li, M. Huang, M. Ma, W. Ye, D.Y. Liu, D.M. Song, B.Z. Bai, and H.S. Fang: *Trans. Nonferr. Met. Soc.*, 2006, vol. 16, pp. 242–53.
46. P.S. Mohanty and J.E. Gruzleski: *Acta Metall. Mater.*, 1995, vol. 43, pp. 2001–12.
47. S.C. Tjong and H. Chen: *Mater. Sci. Eng. R*, 2004, vol. 45, pp. 1–88.
48. X. Liu, Y. Wu, and X. Bian: *J. Alloys Compd.*, 2005, vol. 391, pp. 90–94.
49. L. Yu, X. Liu, H. Ding, and X. Bian: *J. Alloys Compd.*, 2007, vol. 429, pp. 119–25.
50. K. Nogita, S.D. McDonald, K. Tsujimoto, K. Yasuda, and A.K. Dahle: *J. Electron Microsc.*, 2004, vol. 53, pp. 361–69.
51. H. Dai, J. Du, L. Wang, C. Peng, and X. Liu: *Phys. B Condens. Matter*, 2010, vol. 405, pp. 573–78.
52. J. Chang, I. Moon, and C. Choi: *J. Mater. Sci.*, 1998, vol. 33, pp. 5015–23.
53. P.L. Schaffer, D.N. Miller, and A.K. Dahle: *Scripta Mater.*, 2007, vol. 57, pp. 1129–32.
54. V.M. Sreekumar, R.M. Pillai, B.C. Pai, and M. Chakraborty: *Appl. Phys. A Mater. Sci. Process.*, 2008, vol. 90, pp. 745–52.
55. H.T. Li, Y. Wang, and Z. Fan: *Acta Mater.*, 2012, vol. 60, pp. 1528–37.
56. I. Haginoya and T. Fukusako: *Trans. Jpn. Inst. Met.*, 1983, vol. 24, pp. 613–19.
57. E.M. Hinton, W.D. Griffiths, and N.R. Green: *Mater. Sci. Forum*, 2013, vol. 765, pp. 180–84.
58. A. McLeod and C. Gabryel: *Metall. Trans. A*, 1992, vol. 23A, pp. 1279–83.
59. S.H. Oh, Y. Kauffmann, C. Scheu, W.D. Kaplan, and M. Rühle: *Science*, 2005, vol. 310, pp. 661–63.
60. N. Shibata, A. Goto, K. Matsunaga, T. Mizoguchi, S.D. Findlay, T. Yamamoto, and Y. Ikuhara: *Phys. Rev. Lett.*, 2009, vol. 102, p. 136105 (4 pp).
61. T. Hong, J.R. Smith, and D.J. Srolovitz: *Acta Metall. Mater.*, 1995, vol. 43, pp. 2721–30.
62. Z.Y. Fan: *Metall. Mater. Trans. A*, 2013, vol. 44A, pp. 1409–18.
63. B. Bramfitt: *Metall. Trans.*, 1970, vol. 1, pp. 1987–95.
64. R. Schweinfest, S. Köstlmeier, F. Ernst, C. Elsässer, T. Wagner, and M.W. Finnis: *Philos. Mag. A*, 2001, vol. 81, pp. 927–55.
65. D.A. Porter, K.E. Eastering, and M.Y. Sherif: *Phase Transformations in Metals and Alloys*, 3rd ed., CRC Press, Boca Raton, 2009.
66. D.M. Herlach, K. Eckler, A. Karma, and M. Schwarz: *Mater. Sci. Eng. A*, 2001, vols. 304–306, pp. 20–25.
67. M. Schwarz, A. Karma, K. Eckler, and D.M. Herlach: *Phys. Rev. Lett.*, 1994, vol. 73, pp. 1380–83.